ACS APPLIED MATERIALS & INTERFACES

Research Article

www.acsami.org

Effective Electrochemistry of Human Sulfite Oxidase Immobilized on Quantum-Dots-Modified Indium Tin Oxide Electrode

Ting Zeng,[†] Silke Leimkühler,[†] Joachim Koetz,[‡] and Ulla Wollenberger*[,†]

[†]Institute of Biochemistry and Biology and [‡]Institute of Chemistry, University of Potsdam, Karl-Liebknecht-Strasse 24-25, 14476 Potsdam-Golm, Germany

Supporting Information

ABSTRACT: The bioelectrocatalytic sulfite oxidation by human sulfite oxidase (*h*SO) on indium tin oxide (ITO) is reported, which is facilitated by functionalizing of the electrode surface with polyethylenimine (PEI)-entrapped CdS nanoparticles and enzyme. *h*SO was assembled onto the electrode with a high surface loading of electroactive enzyme. In the presence of sulfite but without additional mediators, a high bioelectrocatalytic current was generated. Reference experiments with only PEI showed direct electron transfer and catalytic activity of *h*SO, but these were less pronounced. The application of the polyelectrolyte-entrapped quantum dots (QDs) on ITO electrodes provides a compatible surface for enzyme binding with promotion of electron transfer. Variations of the buffer solution conditions, e.g., ionic strength, pH, viscosity, and the effect of oxygen, were studied in order to understand intramolecular and heterogeneous electron transfer from *h*SO to the electrode. The results are consistent with a model derived for the enzyme by using flash photolysis in solution and spectroelectrochemistry and molecular dynamic simulations of *h*SO on monolayer-modified gold electrodes. Moreover, for the first time a photoelectrochemical electrode involving immobilized *h*SO is demonstrated where photoexcitation of the CdS/*h*SO-modified electrode lead to an enhanced generation of bioelectrocatalytic currents upon sulfite addition. Oxidation starts already at the redox potential of the electron transfer domain of *h*SO and is greatly increased by application of a small overpotential to the CdS/*h*SO-modified ITO.

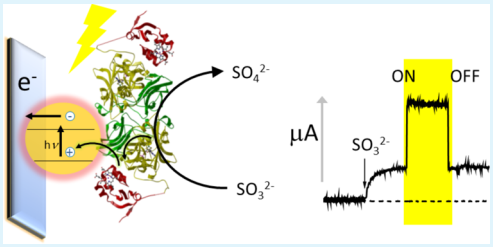

KEYWORDS: *human sulfite oxidase, direct electrochemistry, bioelectrocatalysis, photocurrent, CdS quantum dots*

1. INTRODUCTION

Nanotechnology has gained considerable interest in the field of analytical chemistry in combination with bioanalytical systems in the past two decades. Nanostructured materials exhibit properties markedly different from those of conventional bulk materials mainly because of their unique microstructure.[1] The main factors that influence the mechanical, optical, electric, and magnetic properties of the nanoparticles as well as their chemical reactivity are the surface effect and the size-dependent quantum dot (QD) effect.[2−4] Quantum dots (QDs) are nanocrystalline particles (<10 nm) with unique quantum-confined photonic and electronic properties. In 1998, Nie[5] and Alivisatos[6] demonstrated the potential application of QDs as fluorescent labels. The use of semiconductive QDs to follow biocatalytic events and to establish photobioelectrochemical systems is an active area of research.[7] For example, electrochemistry and photobiocatalysis of enzymes immobilized on semiconductive material for bioelectronic devices,[8−10] detection,[9,11] or artificial photosynthesis[12] were reported. The latter systems use the rectifying properties of the semiconductors to generate directed photocurrents. It was possible to control the direction of the photocurrent by application of a potential and to follow biocatalysis via indication of mediators or via an electroactive product or cosubstrate.[8] The direct reaction of a protein became possible after modification of semiconductor nanoparticles with an appropriate hydrophilic and charged shell.[8,13] To obtain an optically controlled charge transfer from cytochrome c (cyt c) to a gold electrode, CdSe-ZnS QDs were immobilized on the electrode. Only the application of additional anionic surface modifier of the QDs resulted in enhanced photocurrents.[13] Via the combination of cyt c and enzymes on QDs-modified electrodes, photoswitchable bioelectrocatalytic sensors were created, where the electrochemical conversion of cyt c is amplified by the enzyme in the presence of its substrate.[8] However, the enzymes were not directly reacting with the activated nanoparticles. Recently our group and others demonstrated direct unmediated electronic communication of the molybdenum enzyme human sulfite oxidase (*h*SO) to electrodes using gold nanoparticles.[14]

Sulfite oxidases (SO) form one of the three families of mononuclear molybdoenzymes that have been defined on the basis the different active site structures.[15,16] SO from animals generally are homodimers, which consists of an N-terminal heme-containing domain (SO-HD) bonding cyt b5, and a C-terminal domain containing the molybdenum complex cofactor (Moco) and a dimerization site (SO-MD). SO can catalyze the oxidation of sulfite to sulfate, coupled with the subsequent reduction of two equivalents of cyt c.[17,18] This reaction has

Received: July 22, 2015
Accepted: September 10, 2015
Published: September 10, 2015

DOI: 10.1021/acsami.5b06665
ACS Appl. Mater. Interfaces 2015, 7, 21487−21494

Scheme 1. Sketch of the Two Procedures for Modification of Electrodes with PEI-Capped CdS QDs and *h*SO[a]

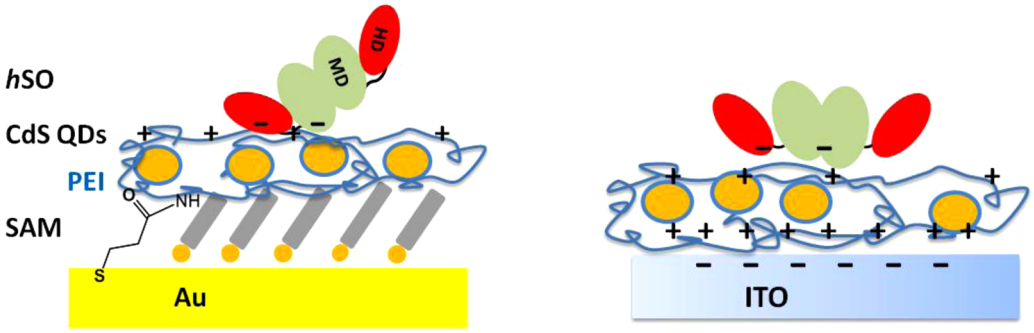

[a]The left picture illustrates electrostatic adsorption of *h*SO to PEI-capped CdS QDs that are covalently linked to the self-assembled DTSP on gold. The modification of ITO (right picture) involves electrostatic adsorption of CdS QDs to the negatively charged ITO followed by adsorption of *h*SO.

been explored for biosensors where cyt c mediated electrons to the electrode using animal SO[19,20] or bacterial sulfite dehydrogenase.[21,22] Direct voltammetry can provide further insights to the enzyme mechanism as was initially demonstrated for chicken SO (*c*SO) on pyrolytic graphite.[23] This work identified the heme of the SO-HD as an inbound relay between the catalytic site and the electrode for the catalytic turnover of *c*SO. Electrodes with the very homologous human enzyme *h*SO were constructed using self-assembled monolayers of amino alkyl thiols[24] or monolayers that have been additionally covered by polycations.[25] Here also the SO-HD acts as a redox relay. Recently we showed that high catalytic currents are also achieved with *h*SO adsorbed to polyethylenimine (PEI) covalently bound to nanostructured gold electrodes.[25] In this connection, small PEI-entrapped Au nanoparticles synthesized in ionic liquids[14,26] and covalently coupled to a monolayer-modified gold electrode enhance direct electron transfer.[14] On such electrodes, pronounced nonturnover currents are observed, and upon substrate addition, large electrocatalytic currents appeared. However, the substrate-dependent signals were still impaired by a parasitic reaction of molecular oxygen.[14,25]

The aim of the present work was to develop a modified electrode that enables very efficient bioelectrocatalysis and photoelectrochemical reaction using direct electronic communication to an enzyme on an activated semiconductor nanoparticle-modified transparent electrode.

For this purpose, PEI-capped CdS QDs are attached to the transparent indium tin oxide (ITO) electrode to assist attachment of *h*SO and to provide a photoactivated functionality. QDs of about 2 nm size were synthesized by a recently developed green synthesis route.[27] The resulting CdS nanoparticles are entrapped by the hyperbranched PEI, containing primary secondary and tertiary amino groups. Electrochemical experiments have been carried out on ITO electrodes in order to achieve efficient heterogeneous and intramolecular electron transfer for *h*SO bioelectrocatalysis and to enable us to investigate the role of CdS QDs and the effect of visible light on the photocurrent response of the biosensor.

2. EXPERIMENTAL SECTION

2.1. Materials. All chemicals were of analytical grade and were used as received. 3,3′-Dithiodipropionic acid di(*N*-hydroxysuccinimide ester) (DTSP) was purchased from TCI (Eschborn, Germany). ITO slides, sodium sulfite, sulfuric acid, and hydrogen tetrachloroaureate were purchased from Sigma-Aldrich (Steinheim, Germany). Tris-(hydroxymethyl) aminomethane (Tris base) was obtained from Serva (Heidelberg, Germany). Nitric acid, potassium dihydrogen phosphate, and dipotassium hydrogen phosphate were from Merck (Darmstadt, Germany). Potassium carbonate and polyethylenglycol 400 (PEG 400) were purchased from Roth (Karlsruhe, Germany). $CdCl_2$ (>99%) and Na_2S (>99%) were obtained from Fluka and used as received. Branched polyethylenimine (PEI, Lupasol G 100 with M_w = 5000 g mol^{-1}) was from BASF (Ludwigshafen, Germany). The solutions were prepared with 18 MΩ Millipore water (Millipore, Eschborn, Germany).

2.2. Expression and Purification of *h*SO. *h*SO was expressed in *Escherichia coli* TP1000 cells containing plasmid pTG718 and was purified following a previously reported protocol.[17]

2.3. Synthesis of Nanoparticles. PEI-capped CdS QDs were synthesized according to the previously reported procedure.[27] Briefly, 0.75 mL of a precooled aqueous 0.5 mM $CdCl_2$ solution was dropwise added to 3 mL of a 1 wt % PEI solution under stirring while the temperature was maintained at 2 °C. After that, the same amount of a precooled aqueous 0.5 mM Na_2S solution was slowly added, and the mixture was stirred for about 5 min. The whole procedure was carried out in a dark environment.

Synthesis of PEI-capped AuNPs in aqueous solution followed the protocol reported by Note et al.[28] Aqueous solutions of 1 wt % PEI and 2 mM $HAuCl_4$ solution were prepared, mixed with 1:1 ratio (w/w) at room temperature, and heated up to 100 °C for 5 min. The generated nanoparticle-containing solution was cooled down to room temperature using a water bath and then kept at 4 °C.

2.4. Characterization of Nanoparticles. PEI-capped CdS nanoparticles (CdS QDs) and AuNPs were characterized by using dynamic light scattering (DLS) at 25 °C at 173° (backscattering technique) with a Nano Zetasizer 3600 (Malvern). The freshly prepared CdS nanoparticles show a maximum of 2.3 nm in the number plot and of 2.7 nm in the intensity plot, indicating that very small PEI-capped QDs are formed. These results are in good agreement with our recently published data in the presence of PEI samples of higher molar mass.[27] By using the above-desribed procedure for making Au nanoparticles,[28] stable PEI-entrapped Au nanoparticles with an Z average of 14.4 ± 0.4 nm are formed. Both freshly prepared aqueous nanoparticle dispersions were used without further treatment in the following electrode fabrication procedure.

2.5. Electrode Fabrication. The two procedures illustrated in Scheme 1 were used for the creation of CdS QDs-modified electrodes. PEI-capped nanoparticles assembled on ITO are based on charge interaction of the polycationic polymer PEI and the negatively charged ITO. The enzyme *h*SO adsorbs to polycationic layer containing the self-assembled nanoparticle/polyelectrolyte layer. The modification of the gold surface includes a self-assembled monolayer (SAM) of DTSP and the cross-linkage between the succinimide active ester and the primary amines of PEI.

2.5.1. Preparation of Modified ITO Electrodes. To clean the surface of the electrodes, the ITO slides were first pretreated in 1 wt % Alconox aqueous solution for at least 30 min, followed by incubation in 70% (v/v) ethanol for 20 min, and two pretreatments in Milli-Q

DOI: 10.1021/acsami.5b06665
ACS Appl. Mater. Interfaces 2015, 7, 21487−21494

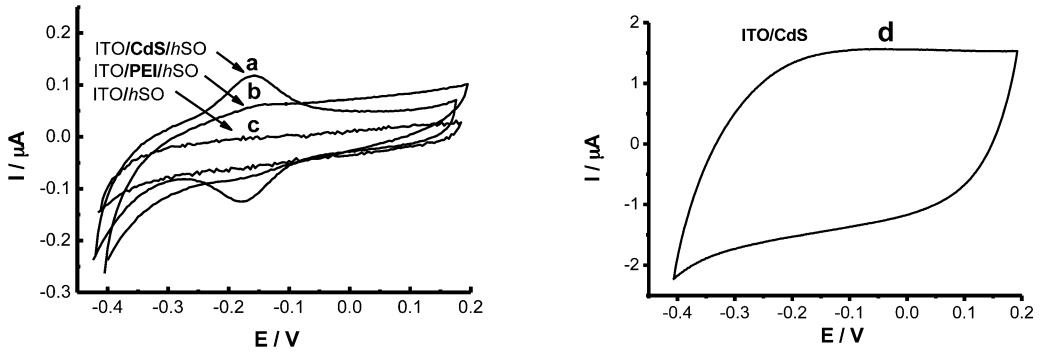

Figure 1. CVs of (a) ITO/CdS/*h*SO, (b) ITO/PEI/*h*SO, (c) ITO/*h*SO, and (d) ITO/CdS electrodes recorded under nonturnover conditions in 750 mM Tris-acetate buffer solution (pH 8.4) saturated with nitrogen. The scan rate is 100 mV s^{-1}.

water each for at least 10 min. Prior to CdS QDs adsorption, the electrodes were equilibrated overnight in 5 mM potassium phosphate buffer at pH 7.0. After drying with a stream of nitrogen gas, 100 μL of 0.5 mM CdS QDs solution was placed onto the conductive surface of the ITO slide and left for at least 2 h at room temperature. The modified electrode (henceforth simply ITO/CdS) was then rinsed with water to remove unabsorbed nanoparticles. For immobilization of *h*SO, 100 μL of freshly prepared 5 μM *h*SO solution (enzyme dissolved in 0.5 mM Tris-acetate solution, pH 7.0) was placed onto the QDs-modified ITO surface for 1 h at 4 °C. The electrodes were subsequently washed with 0.5 mM Tris-acetate buffer solution (pH 7.0). The enzyme-modified electrode, henceforth ITO/CdS/*h*SO, was stored dry at 4 °C when not in use.

The ITO/PEI/*h*SO electrode was fabricated using the same method except that PEI was used instead of the CdS QDs. The ITO/*h*SO electrodes were prepared with omission of either PEI or CdS QDs.

2.5.2. Preparation of Modified Au Electrodes. Gold wires (diameter = 0.5 mm, Goodfellow, Bad Nauheim, Germany) were cleaned as reported by Frasca et al.[14] The cleaned wires were immersed into a 50 mM DTSP solution (DTSP dissolved in DMSO) for 2 h at room temperature for the formation of a self-assembled monolayer on the surface. The DTSP-modified electrodes were then rinsed with DMSO and water and then immersed into 0.2 M K_2CO_3 (pH 10.0) for 20 min in order to activate the surface. Then, the electrodes were incubated in either CdS QDs or AuNPs solution for 1 h at room temperature. Immobilization of *h*SO was achieved by immersion of the NP-modified gold electrode into 0.5 mM Tris-acetate at pH 7.0 containing 2 μM *h*SO at 4 °C for 30 min. The modified electrodes were stored dry at 4 °C when not in use. Before each measurement, the Au/CdS/*h*SO or Au/AuNPs/*h*SO electrodes were thoroughly rinsed with 5 mM Tris-acetate (pH 8.4) to remove enzyme that was not tightly bound.

2.6. Electrochemical Investigations. Electrochemical measurements were carried out using a custom-made 1 mL measuring chamber equipped with a Ag/AgCl/1 M KCl reference electrode and platinum-wire counter electrode. The working electrodes were modified ITO slides or modified Au wires according to the procedure described above. Experiments were carried out at room temperature with a PalmSens potentiostat and analyzed with PSLite 3.0 software (Palmsens, The Netherlands). Scan rates were varied between 0.02 and 3 V s^{-1} to determine surface coverage and electron transfer rate constant. A scan rate of 0.002 V s^{-1} was normally used to record catalytic currents. Amperometric experiments were carried out under constant stirring of the solution and applying a potential of 0 V (vs Ag/AgCl/1 M KCl) to the working electrode. Unless stated otherwise, the electrolyte solutions were purged with nitrogen gas for 30 min to reduce the level of oxygen dissolved before each electrochemical measurement.

The photocurrent measurements are carried out in a 1 mL homemade spectro-electrochemical cell equipped with a quartz window opposite the working electrode, a Ag/AgCl reference electrode, and a Pt counter electrode. The measurements were carried out using photodiodes from Conrad GmbH (Germany) (45 mW LED, 340−700 nm wavelength) mounted at the quartz window. The working potential was 0 V (vs Ag/AgCl/1 M KCl). During amperometric photocurrent measurements, the solution was stirred constantly.

3. RESULTS AND DISCUSSION

3.1. Noncatalytic Voltammetry of *h*SO. PEI-capped CdS QDs-modified ITO surface resulted in pronounced direct electrochemistry of the adsorbed *h*SO. Cationic surface modifiers promote adsorption of SO in a suitable orientation for efficient direct transfer between SO and an electrode.[14,23,24,29] The positively charged surface of CdS QDs, specifically the amino-group-rich PEI, is expected to provide adsorption of *h*SO that facilitate the direct electron transfer reaction.

Figure 1 compares the electrochemical behavior of *h*SO adsorbed to modified ITO electrodes in the presence and absence of CdS nanoparticles. Cyclic voltammograms (CV) recorded on a (stationary) ITO electrode modified with CdS and *h*SO (ITO/CdS/*h*SO) are shown in Figure 1a. A couple of well-defined, nearly symmetric redox peaks were obtained with the formal potential of −157 mV (vs Ag/AgCl in 1 M KCl), which was calculated by averaging the cathodic and anodic peak potentials corresponding to the redox species. In contrast, the CV curve of ITO surface modified only with CdS QDs (Figure 1d) shows an increased capacitance of the surface but does not show any redox peak, which allows the conclusion that the redox signals result from *h*SO. Thus, a direct electron transfer of *h*SO on a PEI-capped-CdS-coated ITO electrode has been achieved successfully. Additionally, a control experiment was carried out with *h*SO directly adsorbed on an ITO surface (Figure 1c). It is obvious that no visible redox peaks evolved at such an electrode surface. The CV of *h*SO on a PEI-modified ITO electrode was additionally measured (Figure 1b), and the response of redox peak is much smaller compared with that of *h*SO immobilized on CdS-modified electrode (Figure 1a). Therefore, we assume that PEI binds *h*SO and CdS nanoparticles that promote the direct electron transfer process between the *h*SO and electrode surface. The peak potential corresponds to values obtained on other electrodes and for the isolated heme domain[14,24] and is therefore ascribed to the reversible one-electron transfer process of *h*SO-HD domain.

CV of ITO/CdS/*h*SO was recorded in 750 mM Tris-acetate buffer at various scan rates (Figure S1a). The shape of the curves is indicative of a reversible one-electron transfer, with the number of transferred electrons $n = 0.92$ estimated from the width at midheight that tends toward $90.6/n$ mV. This value also indicates a very homogeneous distribution of the enzyme.

DOI: 10.1021/acsami.5b06665
ACS Appl. Mater. Interfaces 2015, 7, 21487−21494

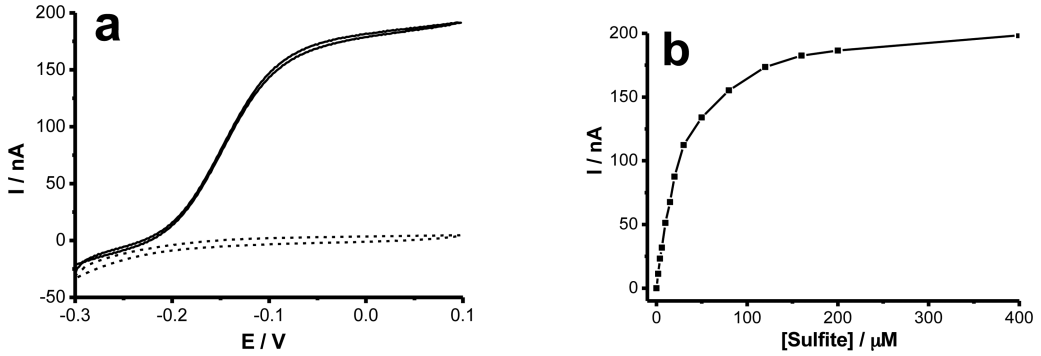

Figure 2. (a) CVs of ITO/CdS/*h*SO at a scan rate of 2 mV s^{-1} in 750 mM Tris-acetate buffer (pH 8.4) (dashed line) and with 200 μM sulfite (solid line). (b) Dependence of the catalytic current on sulfite concentration.

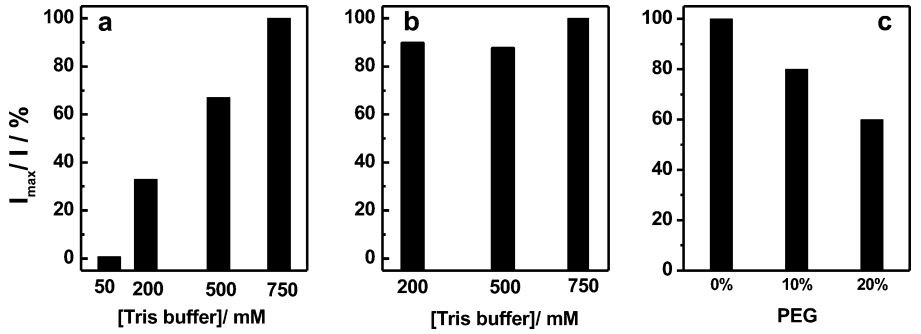

Figure 3. (a) Percent of catalytic current in the presence of 200 μM sulfite related to the catalytic current in 750 mM Tris-acetate buffer with various concentrations of Tris-acetate buffer. (b) Effect of buffer concentration on the noncatalytic reaction. (c) Percent of catalytic current in the presence of 200 μM sulfite related to the catalytic current in the presence of 0, 10, and 20% viscogen PEG 400 and 750 mM Tris-acetate buffer.

Both anodic and cathodic peak currents exhibited a linear dependence on the scan rate in the range from 0.01 up to 1 V s^{-1}, suggesting that *h*SO on ITO/CdS exhibits surface-controlled electrochemical behavior. Only at a higher scan rate above 1 V s^{-1} is a deviation from linearity observed (Figure S1b). This may indicate different electron transfer distances because it has been observed for proteins assembled in multilayers.[30] This is further supported by the fact that the estimated surface coverage (Γ) is lower for the high scan rates compared to that of the lower one (Γ = 2.8 pmol cm^{-2} for 3 V s^{-1} and Γ = 4.2 pmol cm^{-2} for 1 V s^{-1}). Because a noncatalytic signal of *h*SO is clearly observed at the ITO/CdS/*h*SO electrode, the surface concentration of electrochemically active *h*SO was calculated by integration of the reduction peak of the observed CV curve according to the equation[31]

$$\Gamma = I_p 4RT/\nu n^2F^2A$$

where I_p is the peak current of the nonturnover response of the immobilized enzyme at a given scan rate ν, n is the number of electrons transferred, F is the Faraday constant (F = 96 485 C mol^{-1}), and A is the geometric area of the electrode (A = 0.2 cm^2).

We therefore suggest that a prolonged electron transfer is also attributed to a reorientation processes of the *h*SO-HD at the electrode surface.[32] It should be pointed out that the ionic strength was low only during the initial adsorption process and that all the CVs were carried out in 750 mM Tris-acetate buffer concentration, where electrostatic interactions between the positively charged CdS QDs head groups and *h*SO are weak. Because stringent washing does not remove bound enzyme, the binding to the polyelectrolyte-capped QD-modified surface is most likely via interaction of the dimerization domain, as in the case of previously proposed *h*SO-modified gold electrodes.[14,24]

The highest value of electroactive species was calculated to be Γ = 4.2 pmol cm^{-2} for scan rates up to 1 V s^{-1}. The cyt b_5 domain of *h*SO is the electrochemically active species in the nonturnover process. Assuming a footprint of the enzyme being ca. 0.84 × 10^{-12} cm^2 (dimer), the theoretical Γ value for monolayer coverage with the dimer is 1.98 pmol cm^{-2}. This value is close to monolayer coverage of *h*SO on ITO/CdS QDs surface.

The electron transfer rate constant k_s of *h*SO on the modified electrode was calculated from the peak-to-peak potential separation ΔE_p according to Laviron.[33] The electron transfer rate constant k_s was estimated to be 27.1 s^{-1} (Figure S2), which is comparable with the values obtained for *c*SO on alkanethiol-modified gold electrodes[29] and *h*SO on self-assembled amino-terminated monolayers[24] but larger than the values at a AuNP-modified gold electrode.[14] The modification of ITO with CdS entrapped in polycations seem to provide a better interaction with *h*SO and enhancement in electronic communication in contrast to those previously reported for antimony-doped tin oxide.[34] In the latter case, no preferred orientation of the anionic cyt heme domain was provided. Here the amino groups of the capping PEI provide a surface to which *h*SO can assemble in a productive orientation.

3.2. Bioelectrocatalysis of Sulfite Oxidation. The ITO/CdS/*h*SO exhibited clear electrocatalysis of the oxidation of sulfite, which is obvious from the shape of the CVs in the presence of substrate. As shown in Figure 2a, with the addition of sulfite into 750 mM Tris-acetate buffer at pH 8.4, an obvious increase of the oxidation current that starts from −0.25 V appeared, which is a clear indication of the electrocatalytic

DOI: 10.1021/acsami.5b06665
ACS Appl. Mater. Interfaces 2015, 7, 21487−21494

reaction. The inflection point of the electrocatalytic curve coincides with the noncatalytic formal potential of the heme domain and thus also suggests very efficient electrode coupling with no overpotential for the electrocatalysis. No similar phenomena could be observed at the modified electrodes without *h*SO under the same conditions.

From variation of the substrate concentration, it is obvious that the maximum catalytic current value for 750 mM Tris-acetate buffer at pH 8.4 was already reached in the presence of 200 μM sulfite (Figure 2b). The bioelectrocatalysis of *h*SO on modified gold electrodes is strongly dependent on buffer concentration because of the necessity of flexible interaction of the mediating heme b_5 domain of SO with the catalytic molybdenum-containing unit and the electrode.[14,24,35] Therefore, the effect of buffer concentration was studied with the novel assemblies as well. No catalytic current was detected in very low concentration of Tris-acetate buffer (5 mM). However, when increasing buffer concentration (>200 mM), the current density increased dramatically (Figure 3a). In contrast, the noncatalytic current does not show this strong ionic strength dependence (Figure 3b).

Besides the buffer concentration, solution viscosity should also influence the catalytic current and thus deliver another indication of the flexibility of the SO-HD to mediate electrons between the catalytic site and the electrode and of the fact that protein conformational change is involved in the reaction. Figure 3c shows a significant decrease of the catalytic current with increasing amounts of PEG 400. The catalytic current values obtained from these experiments for immobilized *h*SO on ITO/CdS with 10 and 20% (v/v) PEG 400 is only 80 and 60% compared to the response in buffer solution without PEG 400.

The apparent Michaelis–Menten constan K_M^{app} for sulfite is 20 μM (at pH 8.4) and thus is close to the reported value of K_M = 8.25 μM (at pH 8.5) for *h*SO in solution.[36] This allows us to conclude that sulfite has a sufficiently fast access to the active site of enzyme. Under substrate saturation, the limiting current may be related directly to the turnover rate constant k_{cat}[29]

$$k_{cat} = \frac{I_{lim}}{\Gamma_{hSO} AnF}$$

where I_{lim} refers to the maximum catalytic current obtained in an experiment where mass transport is not the rate limiting step. In the present case, the effects of mass transport can be neglected because of stirring of the solution; thus, we can set $I_{lim} = I_{max}$. The values of k_{cat} were calculated from the values of the catalytic currents at 100 mV. If we assume that all redox active enzymes determined from the noncatalytic CV curve are also catalytically active, then the CV measurements revealed an apparent turnover rate of k_{cat}(electrode) = 3.17 s^{-1} in 750 mM Tris-acetate buffer (pH 8.4) solution. This rate is comparable to that of *h*SO immobilized on a roughed Ag electrode modified with a mixed SAM of $C_8(NH_2)/C_6(OH)$ (1:3 M/M) in 750 mM Tris (pH 7.4) reported by Sezer et al.,[24] who obtained turnover rates of 5.3 s^{-1} from CV data. From their SERR experiments results, they have obtained also a lower rate (k_{cat} = 0.76 s^{-1}) using 200 mM Tris (pH 7.4) at the same surface. However, the huge difference between k_{cat} obtained in immobilized state and that obtained in solution suggested that only a small fraction of enzyme bound at the electrode is catalytically active and can provide conformation change for fast intramolecular electron transfer.

For comparison, CdS QDs were bound to gold electrodes using DTSP, and *h*SO was subsequently adsorbed (Scheme 1). Here also clear redox transformation appeared with a similar midpoint potential as on ITO at −157 mV. However, only 33% of the enzyme loading could be reached; consequently, the catalytic current was also lower. Table 1 summarizes comparative studies on either ITO or gold with CdS QDs or AuNPs (Table 1). The immobilization of *h*SO is in all the cases based on interaction with PEI. Therefore, it is not surprising that the formal potential of *h*SO also did not differ between the various modified surfaces; also, a quasi-reversible 1e$^-$ transfer process was indicated. The surface coverage of *h*SO on the studied system (Table 1) calculated from the area under the peaks was highest for ITO/CdS/*h*SO followed by ITO/AuNP/*h*SO and Au/DTSP/AuNP/*h*SO, where on the latter only half of the amount could be bound in electroactive orientation. In contrast, the loading of *h*SO on Au/CdS reached only 33% of the ITO/CdS value. The higher value of surface loading on ITO may result from the surface roughness, which is not considered for the calculation when taking the geometric area. When comparing ITO/CdS and ITO/AuNP, obviously the slightly higher loading also results in a slightly higher catalytic current density. Similarly, the ITO/PEI surface provides lower enzyme loading and less catalytic current. The determined heterogeneous electron transfer rate constants do not differ much between the AuNPs (15 nm) on Au system and ITO/CdS QDs (2.5 nm) and is lowest without nanoparticles. This indicates the promoting effect of nanoparticles on the direct electron transfer (DET).

Table 1. Redox Parameters of *h*SO Immobilized on Different Modified Electrodes[a]

*h*SO on modified surface	E^0 (mV)	k_s (s^{-1})	I_{cat} (μA cm^{-2})[b]	Γ (pmol cm^{-2})[c]
ITO/CdS	157 ± 5	27.1 ± 2.2	1.0 ± 0.10	4.20 ± 0.32
ITO/AuNPs	156 ± 4	22.4 ± 1.8	0.9 ± 0.15	3.90 ± 0.40
ITO/PEI	155	12.2	0.45	1.02
Au/DTSP/CdS	152 ± 4	18.1 ± 2.4	0.65 ± 0.10	1.40 ± 0.20
Au/DTSP/AuNPs	155 ± 6	32.2 ± 1.9	0.95 ± 0.12	2.10 ± 0.15

[a]The data were estimated from CV values determined for 750 mM Tris-acetate buffer, pH 8.4. [b]Catalytic current density in the presence of 200 μM sulfite; scan rate = 2 mV s^{-1}. [c]For Γ calculation, the geometric area was used A(Au) = 0.08 cm^{-2}, and A(ITO) = 0.20 cm^{-2}

In the crystal structure of *c*SO, a distance between the molybdenum and the heme center was determined as 32 Å,[37] which does not allow efficient intramolecular electron transfer (IET). From previous investigation, a conformation change in solution during the catalytic process is reasonable to bring the heme and Mo center much closer.[38] The dependence of the catalytic currents on buffer concentration and the effect of viscosity are consistent with the role of conformational changes on intramolecular electron transfer in *c*SO observed by using flash photolysis as reported by Feng et al.[35] It is important to note that the formal potential of *h*SO-HD is unaffected by the addition of PEG 400; also, the direct heterogeneous electron transfer rate constant k_s was similar to those of the values in the absence of PEG 400. Using molecular dynamic modeling and spectroelectrochemistry, the mechanism on a monolayer-

DOI: 10.1021/acsami.5b06665
ACS Appl. Mater. Interfaces 2015, 7, 21487−21494

modified electrode surface was also proposed to involve domain movement after an initial electrostatic interaction and binding via the dimerization domain.[24,32] Therefore, SO can adopt different conformations by domain movement, which reduces the distance during the catalytic cycle.[23,35,39] From ionic strength and viscosity dependencies, we can furthermore exclude the possibility of a tiny QD bridge between the SO-HD and SO-MD and thus make conformational rearrangements for intramolecular electron transfer obsolete. However, we may propose that the shape of the surface allows high loading and good access for substrate to the active site of enzyme.

3.3. Oxygen Effect. Cyt c is the physiological electron acceptor for mammalian SO.[15] In contrast, for the oxidation of sulfite by plant SO, oxygen acts as the terminal electron acceptor.[40] Furthermore, SO is also capable of transmitting electrons to different electron mediators (e.g., 2,6-dichlorophenol indophenol, ferricyanide, and methylene blue).[41] Molecular oxygen reacts only slowly with the reduced enzyme as well. Therefore, in experiments using AuNPs or simple SAMs, a decrease of catalytic current was observed for measurement in air compared to that under nitrogen atmosphere (Figure 4).

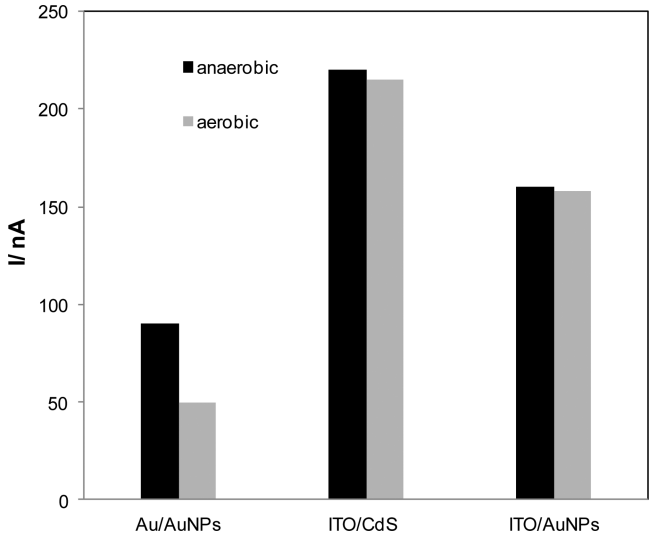

Figure 4. Catalytic current of *h*SO immobilized on different modified electrodes in the presence of 200 μM sulfite in the presence and absence of oxygen. The data were determined by CV at scan rate of 2 mV s^{-1}.

*h*SO on modified Au surface displayed a 40% reduced catalytic current under ambient conditions. The results show that oxygen is also a slow electron acceptor for *h*SO on gold electrode; this causes a sensitivity reduction of catalytic response. Such an influence has not been discussed in earlier papers. However when *h*SO is immobilized on a CdS QDs-modified ITO surface, there is no difference between the catalytic current recorded under aerobic or anaerobic condition (Figure 4). The results indicate a more efficient electron path from immobilized enzyme to the ITO electrode and that oxygen is not a competitive electron acceptor.

3.4. Effect of Light Illumination. We studied the effect of visible light on the electrocatalysis of sulfite by *h*SO/CdS QDs-modified ITO electrode under aerobic conditions. For the analysis of the light-induced effects, amperometric photocurrent measurements were applied. CdS QDs used here have an overall diameter of about 2.5 nm including the CdS core and a thin layer of PEI. The CdS nanoparticles have a band gap of around 2.3 eV. By illumination of the bare ITO and ITO/CdS electrode, no photocurrent appeared in either aerobic or anaerobic conditions. Furthermore, no photocurrent was observed if the ITO or CdS QD-modified electrode (enzyme-free) is illuminated in the presence of substrate.

Thus, sulfite cannot be oxidized at the QD electrode under these conditions. In contrast, for *h*SO on the ITO/CdS QDs surface, the current increased steeply and approached a stationary value after the addition of sulfite as discussed above (dark current, Figure 5). This catalytic current was

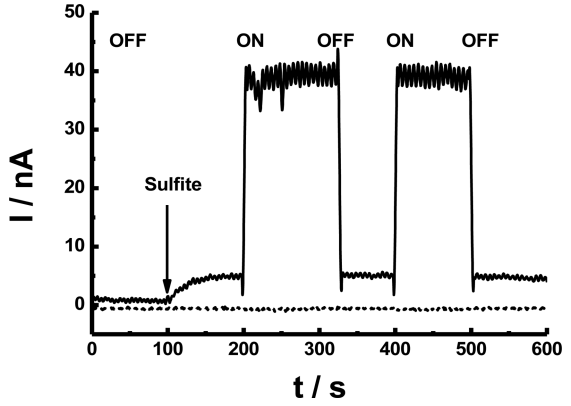

Figure 5. Photocurrent responses of ITO/CdS/*h*SO electrode in 750 mM Tris buffer solution, pH 8.4, in the presence of 400 μM sulfite at 0 V under dark (OFF) and illumination from solution side (ON) (wavelength 470 nm). The dotted line shows the response of the ITO/CdS blank sensor.

several times enhanced under illumination and returned to the dark current level when the light was off. In comparison, the photocurrent produced by ITO/PEI/*h*SO electrode is only 20% higher than that of the dark current. Scheme 2 illustrates the sulfite-dependent photocatalytic ITO/CdS/*h*SO-electrode system.

Scheme 2. Schematic Representation of Visible-Light-Driven Sulfite Oxidation Using *h*SO Adsorbed on CdS QDs Assembled on ITO Electrode[a]

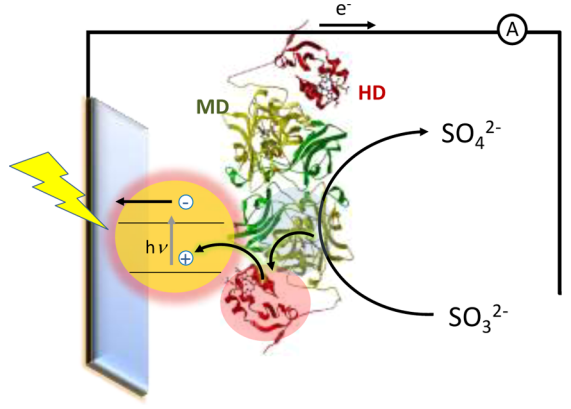

[a]For illustration purposes, the structure of chicken sulfite oxidase (Protein Database: 1SOX) with the HD in red and MD in yellow was used.

DOI: 10.1021/acsami.5b06665
ACS Appl. Mater. Interfaces 2015, 7, 21487−21494

4. SUMMARY AND DISCUSSION

Here we show for molybdoenzyme *h*SO that semiconductor nanoparticles can act as functional units for a photoelectrochemical bioanode with efficient direct electron transfer and thus enable bioelectrocatalytic conversion of its substrate without additional mediator compounds. In comparison to other photoelectrochemical sensors, the direct electronic coupling of hSO and ITO/CdS without additional mediator compounds was possible, and only the addition of the enzyme substrate lead to a measurable current output that is enhanced by photoexcitation. The direct electron communication was observed by immobilizing *h*SO on a positively charged modified ITO electrode. CdS QDs were synthesized in a green synthesis route at low temperatures using hyperbranched PEI as reducing agent and stabilizer as well. From basic characterization by dynamic light scattering, the CdS QDs size is 2−3 nm. PEI is a positively charged polyelectrolyte that binds to the ITO surface and permits *h*SO electrostatic binding. Polycations with primary amino groups can bind electrostatically to the ITO surface, which is rich in electronegative oxygen atoms in In_2O_3 and SnO_2. For example, Schlapak et al. have shown experimentally by X-ray photoelectron spectroscopy the electrostatic attraction between poly(amidoamine) dendrimers and the electronegative oxygen atoms at the ITO surface.[42] The type of linkage between QDs and the ITO surface has an important effect on the properties of the resulting sensor.[43] CdS QDs can further increase the surface coverage and electronic communication of enzyme to the electrode surface compared with those of only PEI. Taking into consideration observation of AuNPs used on gold-wire electrodes, semiconductive CdS QDs-modified ITO surface can provide a suitable microenvironment for *h*SO immobilization (monolayer surface coverage) and facilitate ET (fast-electron-transfer rate constant) when a similar polyelectrolyte is used as capping agent. At a buffer concentration of 750 mM, a rate constant for the direct heterogeneous electron transfer of k_s = 27.1 s^{-1} was obtained for the modified state. The direct noncatalytic signal is assigned to the heme b5 domain of *h*SO as natural redox relay in the enzyme protein in accordance with the literature.[14,24,25] As earlier proposed for other SO-modified electrodes,[23,29] it shuttles between the catalytic active molybdenum center and the modified electrode. The CdS NP-modified surface still provides mobility between the HD and MD, as supported by the decrease of catalytic response at higher viscosity and low ionic strength where the mobility is reduced.[35,38]

It was found that oxygen is not a competitive electron acceptor on this efficient electron communication surface. In contrast, in the unmediated sensor approach with *h*SO on covalently attached PEI-capped AuNPs on Au,[14] molecular oxygen causes reduction of the catalytic current intensity as an indicator of inefficient electronic coupling of immobilized enzyme. In direct comparison to these results, PEI-entrapped semiconductive CdS QDs had a positive influence on the electron transport to the coimmobilized enzyme. In the presence of sulfite, the enhancement of the catalytic current upon photoexcitation indicates that reduction equivalents from the catalytic SO-MD are transferred to the heme b5 domain, which communicates with the QD-modified electrode (Scheme 2). The molybdenum domain is reduced during turnover, and electrons are forwarded to the heme domain of the enzyme. Upon photoexcitation, QD conduction-band electrons were injected into the electrode, and at the same time, heme domain was oxidized by holes from the valence band, permitting electrons to flow again from the catalytic molybdenum site and making it available for the next catalytic turnover. As a result, a biocatalytic photocurrent is measured. The enhancement of the already-observed catalytic current by photoexcitation indicates distribution of nanoparticles−electrode distances and possibly inhomogeneity in enzyme orientation. This is further supported by the deviation of the scan rate dependence of the noncatalytic signal from the linear behavior. At higher scan rates, the sites located further away from the conductive surface cannot be addressed. The ionic strength and viscosity dependency for bioelectrocatalysis oxidation of sulfite shows that tiny QDs do not bridge HD and MD, thus making conformational rearrangements for IET obsolete.

The developed enzyme/nanoparticles assembly on ITO may be of general interest for development of efficient third-generation biosensors and in addition has the potential for fabrication of solar-driven and (photo)electrochemically controlled devices.

■ ASSOCIATED CONTENT

Supporting Information

The Supporting Information is available free of charge on the ACS Publications website at DOI: 10.1021/acsami.5b06665.

Determination of rate constants. (PDF)

■ AUTHOR INFORMATION

Corresponding Author

*E-mail: uwollen@uni-potsdam.de.

Notes

The authors declare no competing financial interest.

■ ACKNOWLEDGMENTS

This work was supported by the Cluster of Excellence "Unifying Concepts in Catalysis" funded by the Deutsche Forschungsgemeinschaft (EXC 314/2), ILB-Brandenburg (80136126), and BMBF (03IS2201B).

■ REFERENCES

(1) Koch, C. C. *Nanostructured Materials: Processing, Properties and Applications*; William Andrew: Norwich, NY, 2006.
(2) Buzea, C.; Pacheco, I. I.; Robbie, K. Nanomaterials and Nanoparticles: Sources and Toxicity. *Biointerphases* **2007**, *2*, MR17.
(3) Roduner, E. Size Matters: Why Nanomaterials Are Different. *Chem. Soc. Rev.* **2006**, *35*, 583−592.
(4) Pokropivny, V.; Skorokhod, V. Classification of Nanostructures by Dimensionality and Concept of Surface Forms Engineering in Nanomaterial Science. *Mater. Sci. Eng., C* **2007**, *27*, 990−993.
(5) Chan, W. C. W.; Nie, S. Quantum Dot Bioconjugates for Ultrasensitive Nonisotopic Detection. *Science* **1998**, *281*, 2016−2018.
(6) Bruchez, M., Jr.; Moronne, M.; Gin, P.; Weiss, S.; Alivisatos, A. P. Semiconductor Nanocrystals as Fluorescent Biological Labels. *Science* **1998**, *281*, 2013−2016.
(7) Medintz, I. L.; Uyeda, H. T.; Goldman, E. R.; Mattoussi, H. Quantum Dot Bioconjugates for Imaging, Labelling and Sensing. *Nat. Mater.* **2005**, *4*, 435−46.
(8) Katz, E.; Zayats, M.; Willner, I.; Lisdat, F. Controlling the Direction of Photocurrents by Means of Cds Nanoparticles and Cytochrome C-Mediated Biocatalytic Cascades. *Chem. Commun.* **2006**, 1395−1397.
(9) Wang, F.; Liu, X.; Willner, I. Integration of Photoswitchable Proteins, Photosynthetic Reaction Centers and Semiconductor/Biomolecule Hybrids with Electrode Supports for Optobioelectronic Applications. *Adv. Mater.* **2013**, *25*, 349−377.

DOI: 10.1021/acsami.5b06665
ACS Appl. Mater. Interfaces 2015, 7, 21487−21494

(10) Chaudhary, Y. S.; Woolerton, T. W.; Allen, C. S.; Warner, J. H.; Pierce, E.; Ragsdale, S. W.; Armstrong, F. A. Visible Light-Driven Co2 Reduction by Enzyme Coupled Cds Nanocrystals. *Chem. Commun.* **2012**, *48*, 58−60.
(11) Yue, Z.; Lisdat, F.; Parak, W. J.; Hickey, S. G.; Tu, L.; Sabir, N.; Dorfs, D.; Bigall, N. C. Quantum-Dot-Based Photoelectrochemical Sensors for Chemical and Biological Detection. *ACS Appl. Mater. Interfaces* **2013**, *5*, 2800−2814.
(12) Bachmeier, A.; Wang, V. C.; Woolerton, T. W.; Bell, S.; Fontecilla-Camps, J. C.; Can, M.; Ragsdale, S. W.; Chaudhary, Y. S.; Armstrong, F. A. How Light-Harvesting Semiconductors Can Alter the Bias of Reversible Electrocatalysts in Favor of H_2 Production and CO_2 Reduction. *J. Am. Chem. Soc.* **2013**, *135*, 15026−15032.
(13) Stoll, C.; Kudera, S.; Parak, W. J.; Lisdat, F. Quantum Dots on Gold: Electrodes for Photoswitchable Cytochrome C Electrochemistry. *Small* **2006**, *2*, 741−743.
(14) Frasca, S.; Rojas, O.; Salewski, J.; Neumann, B.; Stiba, K.; Weidinger, I. M.; Tiersch, B.; Leimkuhler, S.; Koetz, J.; Wollenberger, U. Human Sulfite Oxidase Electrochemistry on Gold Nanoparticles Modified Electrode. *Bioelectrochemistry* **2012**, *87*, 33−41.
(15) Hille, R. The Mononuclear Molybdenum Enzymes. *Chem. Rev.* **1996**, *96*, 2757−2816.
(16) Hille, R. Molybdenum Enzymes Containing the Pyranopterin Cofactor: An Overview. *Metals Ions in Biological System* **2002**, *39*, 187−226.
(17) Temple, C. A.; Graf, T. N.; Rajagopalan, K. V. Optimization of Expression of Human Sulfite Oxidase and Its Molybdenum Domain. *Arch. Biochem. Biophys.* **2000**, *383*, 281−7.
(18) Brody, M. S.; Hille, R. The Kinetic Behavior of Chicken Liver Sulfite Oxidase. *Biochemistry* **1999**, *38*, 6668−77.
(19) Spricigo, R.; Dronov, R.; Rajagopalan, K. V.; Lisdat, F.; Leimkühler, S.; Scheller, F. W.; Wollenberger, U. Electrocatalytically Functional Multilayer Assembly of Sulfite Oxidase and Cytochrome C. *Soft Matter* **2008**, *4*, 972.
(20) Dronov, R.; Kurth, D. G.; Mohwald, H.; Spricigo, R.; Leimkuhler, S.; Wollenberger, U.; Rajagopalan, K. V.; Scheller, F. W.; Lisdat, F. Layer-by-Layer Arrangement by Protein-Protein Interaction of Sulfite Oxidase and Cytochrome C Catalyzing Oxidation of Sulfite. *J. Am. Chem. Soc.* **2008**, *130*, 1122−3.
(21) Rapson, T. D.; Kappler, U.; Hanson, G. R.; Bernhardt, P. V. Short Circuiting a Sulfite Oxidising Enzyme with Direct Electrochemistry: Active Site Substitutions and Their Effect on Catalysis and Electron Transfer. *Biochim. Biophys. Acta, Bioenerg.* **2011**, *1807*, 108−118.
(22) Kalimuthu, P.; Tkac, J.; Kappler, U.; Davis, J. J.; Bernhardt, P. V. Highly Sensitive and Stable Electrochemical Sulfite Biosensor Incorporating a Bacterial Sulfite Dehydrogenase. *Anal. Chem.* **2010**, *82*, 7374−7379.
(23) Elliott, S. J.; McElhaney, A. E.; Feng, C. J.; Enemark, J. H.; Armstrong, F. A. A Voltammetric Study of Interdomain Electron Transfer within Sulfite Oxidase. *J. Am. Chem. Soc.* **2002**, *124*, 11612−11613.
(24) Sezer, M.; Spricigo, R.; Utesch, T.; Millo, D.; Leimkuehler, S.; Mroginski, M. A.; Wollenberger, U.; Hildebrandt, P.; Weidinger, I. M. Redox Properties and Catalytic Activity of Surface-Bound Human Sulfite Oxidase Studied by a Combined Surface Enhanced Resonance Raman Spectroscopic and Electrochemical Approach. *Phys. Chem. Chem. Phys.* **2010**, *12*, 7894−7903.
(25) Zeng, T.; Pankratov, D.; Falk, M.; Leimkühler, S.; Shleev, S.; Wollenberger, U. Miniature Direct Electron Transfer Based Sulphite/Oxygen Enzymatic Fuel Cells. *Biosens. Bioelectron.* **2015**, *66*, 39−42.
(26) Dolya, N.; Rojas, O.; Kosmella, S.; Tiersch, B.; Koetz, J.; Kudaibergenov, S. One-Pot" in Situ Formation of Gold Nanoparticles within Poly(Acrylamide) Hydrogels. *Macromol. Chem. Phys.* **2013**, *214*, 1114−1121.
(27) Kosmella, S.; Venus, J.; Hahn, J.; Prietzel, C.; Koetz, J. Low-Temperature Synthesis of Polyethyleneimine-Entrapped CdS Quantum Dots. *Chem. Phys. Lett.* **2014**, *592*, 114−119.
(28) Note, C.; Kosmella, S.; Koetz, J. Poly(Ethyleneimine) as Reducing and Stabilizing Agent for the Formation of Gold Nanoparticles in W/O Microemulsions. *Colloids Surf., A* **2006**, *290*, 150−156.
(29) Ferapontova, E. E.; Ruzgas, T.; Gorton, L. Direct Electron Transfer of Heme- and Molybdopterin Cofactor-Containing Chicken Liver Sulfite Oxidase on Alkanethiol-Modified Gold Electrodes. *Anal. Chem.* **2003**, *75*, 4841−4850.
(30) Beissenhirtz, M. K.; Scheller, F. W.; Stöcklein, W. F.; Kurth, D. G.; Möhwald, H.; Lisdat, F. Electroactive Cytochrome C Multilayers within a Polyelectrolyte Assembly. *Angew. Chem., Int. Ed.* **2004**, *43*, 4357−4360.
(31) Prodromidis, M. I.; Florou, A. B.; Tzouwara-Karayanni, S. M.; Karayannis, M. I. The Importance of Surface Coverage in the Electrochemical Study of Chemically Modified Electrodes. *Electroanalysis* **2000**, *12*, 1498−1501.
(32) Utesch, T.; Sezer, M.; Weidinger, I. M.; Mroginski, M. A. Adsorption of Sulfite Oxidase on Self-Assembled Monolayers from Molecular Dynamics Simulations. *Langmuir* **2012**, *28*, 5761−5769.
(33) Laviron, E. General Expression of the Linear Potential Sweep Voltammogram in the Case of Diffusionless Electrochemical Systems. *J. Electroanal. Chem. Interfacial Electrochem.* **1979**, *101*, 19−28.
(34) Frasca, S.; Molero Milan, A.; Guiet, A.; Goebel, C.; Pérez-Caballero, F.; Stiba, K.; Leimkühler, S.; Fischer, A.; Wollenberger, U. Bioelectrocatalysis at Mesoporous Antimony Doped Tin Oxide Electrodes—Electrochemical Characterization and Direct Enzyme Communication. *Electrochim. Acta* **2013**, *110*, 172−180.
(35) Feng, C.; Kedia, R. V.; Hazzard, J. T.; Hurley, J. K.; Tollin, G.; Enemark, J. H. Effect of Solution Viscosity on Intramolecular Electron Transfer in Sulfite Oxidase. *Biochemistry* **2002**, *41*, 5816−5821.
(36) Wilson, H. L.; Wilkinson, S. R.; Rajagopalan, K. The G473d Mutation Impairs Dimerization and Catalysis in Human Sulfite Oxidase. *Biochemistry* **2006**, *45*, 2149−2160.
(37) Kappler, U.; Bennett, B.; Rethmeier, J.; Schwarz, G.; Deutzmann, R.; McEwan, A. G.; Dahl, C. Sulfite: Cytochrome C Oxidoreductase Fromthiobacillus Novellus Purification, Characterization, and Molecular Biology of a Heterodimeric Member of the Sulfite Oxidase Family. *J. Biol. Chem.* **2000**, *275*, 13202−13212.
(38) Pacheco, A.; Hazzard, J. T.; Tollin, G.; Enemark, J. H. The Ph Dependence of Intramolecular Electron Transfer Rates in Sulfite Oxidase at High and Low Anion Concentrations. *JBIC, J. Biol. Inorg. Chem.* **1999**, *4*, 390−401.
(39) Kappler, U.; Bailey, S. Molecular Basis of Intramolecular Electron Transfer in Sulfite-Oxidizing Enzymes Is Revealed by High Resolution Structure of a Heterodimeric Complex of the Catalytic Molybdopterin Subunit and a C-Type Cytochrome Subunit. *J. Biol. Chem.* **2005**, *280*, 24999−25007.
(40) Hänsch, R.; Lang, C.; Riebeseel, E.; Lindigkeit, R.; Gessler, A.; Rennenberg, H.; Mendel, R. R. Plant Sulfite Oxidase as Novel Producer of H_2O_2 Combination of Enzyme Catalysis with a Subsequent Non-Enzymatic Reaction Step. *J. Biol. Chem.* **2006**, *281*, 6884−6888.
(41) Cohen, H. J.; Fridovich, I. Hepatic Sulfite Oxidase the Nature and Function of the Heme Prosthetic Groups. *J. Biol. Chem.* **1971**, *246*, 367−373.
(42) Schlapak, R.; Armitage, D.; Saucedo-Zeni, N.; Latini, G.; Gruber, H. J.; Mesquida, P.; Samotskaya, Y.; Hohage, M.; Cacialli, F.; Howorka, S. Preparation and Characterization of Dense Films of Poly (Amidoamine) Dendrimers on Indium Tin Oxide. *Langmuir* **2007**, *23*, 8916−8924.
(43) Khalid, W.; El Helou, M.; Murböck, T.; Yue, Z.; Montenegro, J.-M.; Schubert, K.; Göbel, G.; Lisdat, F.; Witte, G.; Parak, W. J. Immobilization of Quantum Dots Via Conjugated Self-Assembled Monolayers and Their Application as a Light-Controlled Sensor for the Detection of Hydrogen Peroxide. *ACS Nano* **2011**, *5*, 9870−9876.

DOI: 10.1021/acsami.5b06665
ACS Appl. Mater. Interfaces 2015, 7, 21487−21494